mL of bromoform, and the reaction was stirred for 1 h. The solvent was removed in vacuo, and the crude product was purified by preparative thin-layer chromatography (2000-μm silica gel on a 20 × 20 cm^2 glass plate, 5:1 hexane:THF eluent). Yield of Tp'Rh(Br)(d_5-Ph)(CN-neopentyl) (**6**): 40 mg (70%) of white solid.

To a solution of 40 mg (0.0607 mmol) of **6** in 3 mL of THF at 25 °C was added dropwise 0.5 mL of a 0.34 M solution of sodium bis(methoxyethoxy)aluminum hydride (Red-Al) in toluene. The resulting reaction mixture was stirred for 1 h, and then 7 mL of hexanes was added. The reaction was filtered twice through a 1 cm deep plug of silica gel in a 2.5 cm diameter fritted-glass funnel using vacuum. The silica was rinsed with 5 mL of a 5:1 hexanes:THF solvent mixture, and the combined filtrates were evaporated in vacuo to give 30 mg (85% from **6**; 60% from **5**) of the desired product **1**-d_5 as a white solid. ^{1}H NMR (C_6D_6): δ −13.650 (d, J = 24 Hz, 1 H, Rh−H), 0.604 (s, 9 H, $C(CH_3)_3$), 1.896 (s, 3 H, pz CH_3), 2.196 (s, 3 H, pz CH_3), 2.130 (s, 3 H, pz CH_3), 2.246 (s, 3 H, pz CH_3), 2.342 (s, 3 H, pz CH_3), 2.441 (s, 3 H, pz CH_3), 2.741 (s, 2 H, NCH_2), 5.540 (s, 1 H, pz H), 5.708 (s, 1 H, pz H), 5.844 (s, 1 H, pz H). No resonances were observed in the region between δ 6.9 and δ 8.1.

Thermolysis of 1-d_5 in Tetrahydrofuran. A solution of 20 mg of Tp'Rh(H)(d_5-Ph)(CN-neopentyl) (**1**-d_5) in 0.5 mL of THF-d_8 was added to a 5-mm NMR tube containing a ground-glass joint and a Teflon-sealed vacuum-line adapter. The solution was freeze-pump-thawed on a vacuum line and the tube flame-sealed under 1 atm of nitrogen. The sample was heated at 60 °C in an oven and removed every 30 min in order to obtain a ^{1}H NMR spectrum at −40 °C in a cooled NMR probe. The decrease in the integration of the hydride resonance at δ −14.260 along with the increase in the phenyl resonances at δ 6.484 (ortho), δ 6.558 (meta), δ 6.684 (para), δ 6.801 (meta'), and δ 7.619 (ortho') vs an internal standard of silicon grease (δ 0.38) was monitored for a total time of 330 min. Additional spectra were acquired at 768, 1143, and 1683 min, after which time it was concluded that the reaction had reached equilibrium. Data from this experiment was used to generate the plot in Figure 6. The area of the hydride resonance was plotted as ln $((A_t - A_{eq})/(A_0 - A_{eq})) = -k_{obs}t$, and the areas of the phenyl singlets were plotted as ln $(1 - A_t/A_{eq}) = -k_{obs}t$ in determining the rate constants reported in Table V. The approach to equilibrium described in eq 6 can

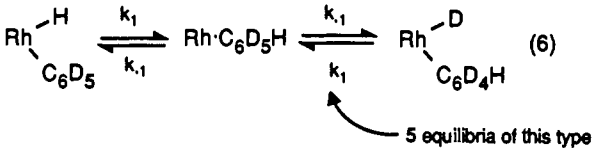

(6)

be evaluated explicitly, using a steady-state assumption on the intermediate and neglecting isotope effects, showing that $k_{obs} = k_1$.

In a second part to this experiment, the tube was broken open and the solution was placed in a second sealed NMR tube along with 50 μL of benzene-d_6. This solution was heated as before, and the integrations of the hydride resonance and phenyl resonances of the isotopomers of **1**-d_5 were monitored every 30 min for 240 min. No significant change in the integrations of the resonances occurred over this time period, and no formation of free benzene-d_5 was observed. Further heating for 15 h did not result in any change.

Thermolysis of 1-d_5 in Toluene-d_8. A sample of **1**-d_5 was prepared in toluene-d_8 and heated at 60 °C as described above. The changes in the integrations of resonances at δ −13.610, 6.911, 7.284, and 8.080 were monitored every 30 min for a total of 330 min. It was not possible to monitor the change in integration for two of the phenyl isomers of **1**-d_5 because they were obscured by residual toluene resonances. The hydride integration data were used to determine k as described above.

Acknowledgment is made to the U.S. Department of Energy (Grant DE-FG02-86ER13569) for support of this work.

Mechanisms for the Reactions between Methane and the Neutral Transition Metal Atoms from Yttrium to Palladium

Margareta R. A. Blomberg,* Per E. M. Siegbahn, and Mats Svensson

Contribution from the Institute of Theoretical Physics, University of Stockholm, Vanadisvägen 9, S-11346 Stockholm, Sweden. *Received October 24, 1991*

Abstract: Calculations including electron correlations have been performed for the oxidative addition reactions between methane and the whole sequence of second row transition metal atoms from yttrium to palladium. The lowest barrier for the C−H insertion reaction is found for the rhodium atom. Palladium has the lowest methane elimination barrier. The barrier height is governed by two factors. In the reactant channel low repulsion favors a low barrier, and in the product channel strong bond formation is important. The atomic state with lowest repulsion toward methane is the d^{n+2} state and the strongest bonds are formed to the d^{n+1} s state. For rhodium both these states are energetically low lying. Only palladium has a bound η^2 precursor state on the ground state potential surface. Another interesting result is that the potential surface for the reaction between methane and the rhodium atom is remarkably similar to the potential surface for the reaction between methane and $ClRhL_2$, which has been studied experimentally.

I. Introduction

Selective C−H activation of saturated alkanes by transition metal catalysts is an important step in the transformation of the abundant, but inert alkanes to more useful products. Therefore a large number of studies, both experimental and theoretical have been performed to elucidate the mechanisms of C−H activation by transition metal complexes. In the present study the reactivity of the second row transition metals with methane is investigated. It is the first study where such a systematic comparison between a whole row of metals has been performed for all the steps in a chemical reaction. The comparison between a wide range of different metals has been found to be essential for the understanding of the factors determining the energetics of the reaction.

Two fundamentally different mechanisms for transition metal activation of hydrocarbon C−H bonds in solution have been established by experiment: (1) oxidative addition to a coordinatively unsaturated metal center and (2) σ-bond metathesis to a metal alkyl or hydride. The present study is concerned with the oxidative addition mechanism. Only a few transition metals are represented among those metal complexes which have been observed to insert into C−H bonds in saturated hydrocarbons via an oxidative addition mechanism. The first observations of alkane C−H insertion in solution were made in 1982 for iridium complexes, where the active intermediates were believed to be coordinatively unsaturated fragments of the general formula Cp*IrL (L = CO, PR_3).[1,2] Shortly afterwards the analogous rhodium fragment (Cp*RhL)

(1) (a) Janowicz, A. H.; Bergman, R. G. *J. Am. Chem. Soc.* **1982**, *104*, 352. (b) Janowicz, A. H.; Bergman, R. G. *J. Am. Chem. Soc.* **1983**, *105*, 3929.

(2) (a) Hoyano, J. K.; Graham, W. A. G. *J. Am. Chem. Soc.* **1982**, *104*, 3723. (b) Hoyano, J. K.; McMaster, A. D.; Graham, W. A. G. *J. Am. Chem. Soc.* **1983**, *105*, 7190.

0002-7863/92/1514-6095$03.00/0

was also found to be active[3] and later on also the $ClRhL_2$ (L = PPh_3) fragment.[4] Other metals proved to be effective in alkane oxidative addition by metal complexes are iron, rhenium, and osmium.[5] Furthermore, the Cp*ML (M = Ir, Rh) and CpML (M = Ir, Rh) fragments have been shown to insert into methane and other alkane C–H bonds in matrices at low temperature (10–20 K).[6-8] Apparently rhodium is the only second row metal active in homogeneous oxidative addition to alkanes, and an important question to answer is why rhodium is more efficient in this process than the rest of the second row metals.

In the present paper the oxidative addition of naked second row transition metal atoms to methane (eq 1) is studied. The reaction

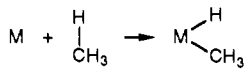

(1)

energy and barrier height of reaction 1 is calculated. From several experimental investigations on both iridium and rhodium complexes it has been inferred that a molecularly bound metal–alkane intermediate is formed in the C–H activation reaction[9-11] and for this reason this type of a molecularly bound complex was also studied for all metal atoms. From a theoretical viewpoint the study of the reactivity of naked metal atoms rather than more realistic ligated complexes is a computational advantage. However, the reactivity of different naked metal atoms is also of interest as such, since this type of information allows a detailed understanding of the basic reaction mechanisms for C–H activation. This type of information is also relevant for the reactivity of ligated complexes, since the different contributions to the reactivity of the metal complexes can be isolated and understood, piece by piece.

The reactivity of naked metal atoms has also been studied experimentally. Recently measurements of reactivities of neutral metal atoms have been performed,[12-14] whereas earlier studies were mainly concerned with the reactivities of metal cations. The reactivity of transition metal cations with hydrocarbons has been studied intensively during the last decades.[15-17] One difference between the neutrals and the ions is that the metal ion has a long-range interaction with the polarizable alkane via the charge-induced dipole force. This attraction is believed to be strong enough to overcome the barrier for metal insertion into the alkane C–H bond that hinders the reactions of the neutral systems.[16-18] Thus the oxidative addition to C–H bonds of alkanes is expected to be more facile for cations than for neutral metal atoms. A comparison of the potential surfaces for methane activation by

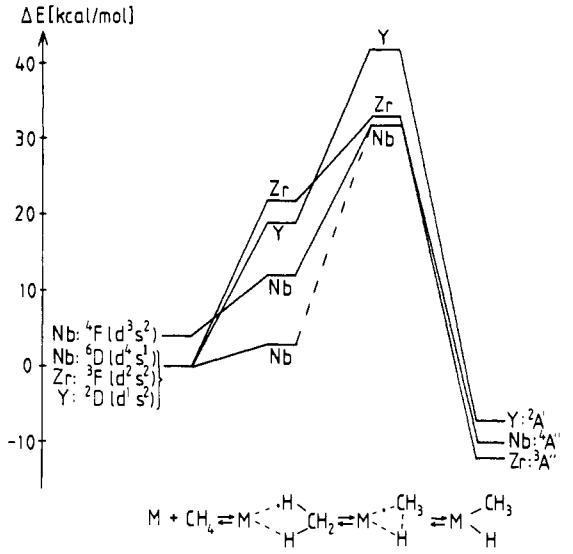

Figure 1. Calculated reaction energies for the insertion of Nb, Zr, and Y into the C–H bond of methane. CH_4 + the ground state of the metal atom is used as reference point. The lowest excited atomic state of the same spin as the insertion product is also marked, and solid lines are drawn for the spin-allowed potential surfaces. The energies in the η^2-region are calculated for the geometry taken from the low-spin rhodium η^2-complex.

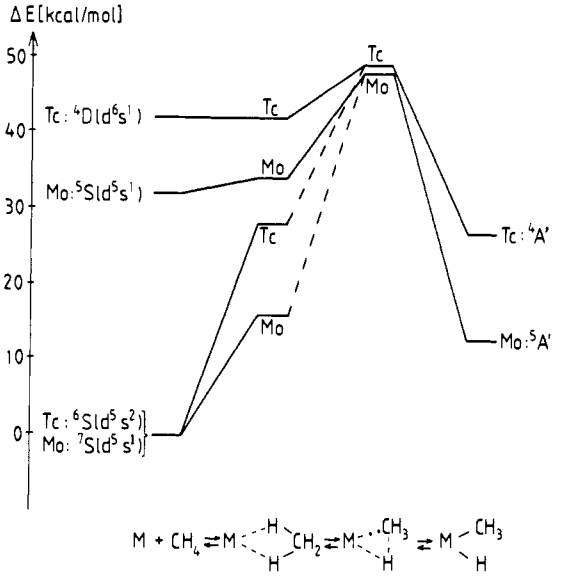

Figure 2. Same as Figure 1 for Tc and Mo.

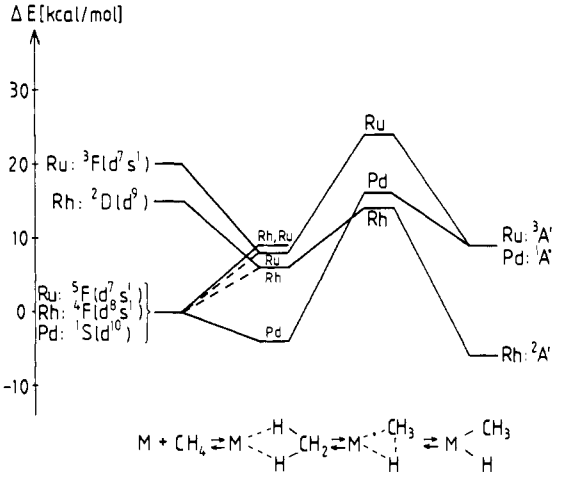

Figure 3. Same as Figure 1 for Ru, Rh, and Pd.

(3) Jones, W. D.; Feher, F. J. *J. Am. Chem. Soc.* **1982**, *104*, 4240.
(4) Sakakura, T.; Sodeyama, T.; Sasaki, K.; Wada, K.; Tanaka, M. *J. Am. Chem. Soc.* **1990**, *112*, 7221.
(5) *Perspectives in the Selective Activation of C–H and C–C Bonds in Saturated Hydrocarbons*; Meunier, B., Chaudret, B., Eds.; Scientific Affairs Division-NATO: Brussels, 1988.
(6) Rest, A. J.; Whitwell, I.; Graham, W. A. G.; Hoyano, J. K.; McMaster, A. D. *J. Chem. Soc., Chem. Commun.* **1984**, 624.
(7) Haddleton, D. M.; McCamley, A.; Perutz, R. N. *J. Am. Chem. Soc.* **1988**, *110*, 1810.
(8) Belt, S. T.; Grevels, F.-W.; Klotzbücher, W. E.; McCamley, A.; Perutz, R. N. *J. Am. Chem. Soc.* **1989**, *111*, 8373.
(9) Buchanan, J. M.; Stryker, J. M.; Bergman, R. G. *J. Am. Chem. Soc.* **1986**, *108*, 1537.
(10) Periana, R. A.; Bergman, R. G. *J. Am. Chem. Soc.* **1986**, *108*, 7332.
(11) Weiller, B. H.; Wasserman, E. P.; Bergman, R. G.; Moore, C. B.; Pimentel, G. C. *J. Am. Chem. Soc.* **1989**, *111*, 8288.
(12) (a) Klabunde, K. J.; Tanaka, Y. *J. Am. Chem. Soc.* **1983**, *105*, 3544. (b) Klabunde, K. J.; Jeong, G. H.; Olsen, A. W. In *Selective Hydrocarbon Activation: Principles and Progress*; Davies, J. A., Watson, P. L., Greenberg, A., Liebman, J. F., Eds.; VCH Publishers: New York, 1990; pp 433–466.
(13) Ritter, D.; Weisshaar, J. C. *J. Am. Chem. Soc.* **1990**, *112*, 6425.
(14) Mitchell, S. A.; Hackett, P. A. *J. Chem. Phys.* **1990**, *98*, 7822.
(15) Weisshaar, J. C. *Adv. Chem. Phys. 81.*
(16) Armentrout, P. B.; Beauchamp, J. L. *Acc. Chem. Res.* **1989**, *22*, 315.
(17) Armentrout, P. B. In *Selective Hydrocarbon Activation: Principles and Progress*; Davies, J. A., Watson, P. L., Greenberg, A., Liebman, J. F., Eds.; VCH Publishers: New York, 1990; pp 467–533.
(18) van Koppen, P. A. M.; Bowers, M. T.; Beauchamp, J. L.; Dearden, D. V. In *Bonding Energetics in Organometallic Compounds*; Marks, T. J., Ed.; ACS Symposium Series: Washington DC, 1990; pp 34–54.

Table I. Calculated Energies (in kcal/mol) Relative to the Ground State of the Metal Atom and Free Methane

metal	ground state	η^2-complex[a]		transition state		insertion product	
		state	ΔE	state	ΔE	state	ΔE
Y	^2D	$^2A_1$	19	$^2A'$	42	$^2A'$	−7
Zr	^3F	$^3A_2$	22	$^3A''$	33	$^3A''$	−12
Nb	^6D	$^6A_1$	3	$^4A''$	32	$^4A''$	−10
		$^4A_1$	12				
Mo	^7S	$^7A_1$	16	$^5A'$	48	$^5A'$	13
		$^5A_1$	34				
Tc	^6S	$^6A_1$	28	$^4A'$	49	$^4A'$	27
		$^4B_1$	42				
Ru	^5F	$^3A_1$	8	$^3A'$	24	$^3A'$	9
		$^5B_2$	9				
Rh	^4F	$^2A_2$	6	$^2A'$	14	$^2A'$	−5
		$^4A_1$	9				
Pd	^1S	$^1A_1$	−4	$^1A'$	16	$^1A'$	9

[a] The energy of the η^2-complex is for all metals calculated in the geometry optimized for the low-spin rhodium η^2-complex.

Table II. Calculated and Experimental Excitation Energies to the Lowest Metal Atomic State with the Same Spin as the Insertion Product (in kcal/mol)

	ground state	low-spin state	ΔE (calc)	ΔE (exp)
Nb	$s^1d^4(^6D)$	$s^2d^3(^4F)$	3.7	4.2
Mo	$s^1d^5(^7S)$	$s^1d^5(^5S)$	32.0	30.8
Tc	$s^2d^5(^6S)$	$s^1d^6(^4D)$	41.7	31.7
Ru	$s^1d^7(^5F)$	$s^1d^7(^3F)$	19.8	18.0
Rh	$s^1d^8(^4F)$	$d^9(^2D)$	14.6	8.1

the neutrals and the cations will be made in a forthcoming paper.[19]

Alkane activation by homogeneous transition metal compounds has been studied theoretically in several previous papers.[20-29] One of the main conclusions from these studies and also from the experimental studies mentioned above[15-18] is that the spectrum of the metal atom or cation to a large extent determines the energetics of the interaction with the hydrocarbons. However, the whole potential surface for the oxidative addition reaction has been studied only for a few different metals previously. Therefore, particularly the factors that determine the height of the barrier for the reaction and the conditions for the occurrence of a precursor species are not well established. The purpose of the present paper is to contribute to the elucidation of these factors by studying the potential surface for C–H insertion for a whole row of transition metals.

The calculations are performed using large atomic basis sets. All valence electrons are correlated using size consistent methods, and relativistic effects are taken into account by means of perturbation theory. The methods and basis sets used are further described in the Appendix, where also the choice of geometries are discussed. On the basis of previous experience[24,25] the present choice of methods, basis sets, and geometries are not expected to lead to errors of more than a few kcal/mol for relative energies.

II. Results

In this section the results for the individual metals will be presented in the form of potential curves for the reaction 1, see Figures 1–3. Four regions on the potential surfaces are investigated: the metal atom plus free methane **1**, a molecular precursor complex with the η^2-structure **2** taken from ref 25, the transition state **3**, and the insertion product $MHCH_3$ complex **4**. The energies in Table I are given relative to the ground state of the metal atom, which in many cases does not have the same spin state as the product complex **4**. Therefore, the lowest atomic state with the same spin as the product is also calculated (see Table II) and marked in the figures. For the η^2-complex **2** two different spin states are investigated for most cases, one corresponding to the atomic ground state and one corresponding to the product complex **4**. The spin-allowed potential surfaces are drawn as solid lines in the figures.

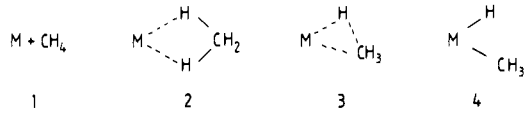

Before the presentation of the results for the individual atoms a few words should be said about the general results for the electronic structure at different parts of the potential surfaces. In the product complex **4** two covalent bonds are formed, and the bonding electron configuration on the metal therefore has to have two open shells. The main bonding atomic configuration for the systems studied here is found to be $4d^{n+1}5s^1$, i.e., the two covalent bonds are formed by one 5s and one 4d electron from the metal. The corresponding state on the atom with the lowest energy will have a high spin coupling of these two electrons, which will often be referred to as the high-spin state below, while the product complex will be referred to as the low-spin state. To the left in the periodic table the $4d^n5s^2$ state will have the same spin as the product complex and will therefore contribute to the bonding. To the right in the periodic table it is the $4d^{n+2}$ state which has the same spin as the product complex and will therefore contribute to the bonding.

The barrier for the reaction between methane and the transition metal atoms is a result of a crossing between two surfaces. Therefore the energy in the transition state region **3** is determined by two important factors. Before the barrier the C–H bond starts to break and methane prepares for the bonding toward the metal. In this region the interaction between methane and the metal atom is essentially repulsive, and the metal adopts the state which is least repulsive. Since the 5s electrons are the most diffuse electrons in the metal, the lower the number of 5s electrons in the configuration the smaller is the repulsion. Therefore the configurations with zero 5s electrons give the lowest repulsion. For the low-spin coupled state with one 5s electron, the repulsion can also be reduced by the formation of two sd hybrids, one pointing toward the C–H bond and the other perpendicular to the line connecting the metal with the C–H bond. By placing two electrons in the latter of these, rather than one in each, the repulsion is significantly decreased. After the barrier the two bonds are formed, and the strength of the bonding in the product complex determines this part of the potential surface. The barrier height for the addition reaction is thus reduced both by a low repulsion in the entrance region and by strong bond formation in the product region.

In the region of the η^2-complex **2** a low-lying $4d^{n+2}$ state is crucial to reduce the repulsion. The bonding force is achieved by an admixture of the low-spin coupled $4d^{n+1}5s^1$ state, which by means of the sd hybridization discussed above, causes a distortion of the electron distribution around the metal atom. Through this distortion the metal nucleus is partly unshielded, and the electrons in the C–H bond will experience an attractive force. It is therefore important that both the $4d^{n+2}$ and the $4d^{n+1}5s^1$ states are low-lying for obtaining bound η^2-complexes. It should be noted that the calculations in this region of the potential surfaces are performed for one single geometry for all metals, the one optimized for the

(19) Blomberg, M. R. A.; Siegbahn, P. E. M.; Svensson, M. to be published.
(20) Blomberg, M.; Brandemark, U.; Pettersson, L.; Siegbahn, P. *Int. J. Quantum Chem.* **1983**, *23*, 855.
(21) Blomberg, M. R. A.; Brandemark, U.; Siegbahn, P. E. M. *J. Am. Chem. Soc.* **1983**, *105*, 5557.
(22) (a) Low, J. J.; Goddard III, W. A. *J. Am. Chem. Soc.* **1984**, *106*, 8321. (b) Low, J. J.; Goddard III, W. A. *Organometallics* **1986**, *5*, 609. (c) Low, J. J.; Goddard III, W. A. *J. Am. Chem. Soc.* **1984**, *106*, 6928. (d) Low, J. J.; Goddard III W. A. *J. Am. Chem. Soc.* **1986**, *108*, 6115.
(23) Blomberg, M. R. A.; Schüle, J.; Siegbahn, P. E. M. *J. Am. Chem. Soc.* **1989**, *111*, 6156.
(24) Blomberg, M. R. A.; Siegbahn, P. E. M.; Nagashima, U.; Wennerberg, J. *J. Am. Chem. Soc.* **1991**, *113*, 476.
(25) Blomberg, M. R. A.; Siegbahn, P. E. M.; Svensson, M. *J. Phys. Chem.* **1991**, *95*, 4313.
(26) Blomberg, M. R. A.; Siegbahn, P. E. M.; Svensson, M. *New J. Chem.* **1991**, *15*, 727.
(27) Koga, N.; Morokuma, K. *J. Phys. Chem.* **1990**, *94*, 5454.
(28) Ziegler, T.; Tschinke, V.; Fan, L.; Becke, A. D. *J. Am. Chem. Soc.* **1989**, *111*, 9177.
(29) Rosi, M.; Bauschlicher, C. W., Jr.; Langhoff, S. R.; Partridge, H. *J. Phys. Chem.* **1990**, *94*, 8656.

Table III. Charge and 4d Population on the Metal Atoms Using the Mulliken Population Analysis

	η^2-complex[a]			transition state			insertion product		
	state	q_M	4d	state	q_M	4d	state	q_M	4d
Y	$^2A_1$	−0.3	1.3	$^2A'$	+0.1	1.3	$^2A'$	+0.5	1.0
Zr	$^3A_2$	−0.3	2.4	$^3A''$	+0.1	2.6	$^3A''$	+0.5	2.3
Nb	$^6A_1$	−0.1	4.2	$^4A''$	+0.1	3.9	$^4A''$	+0.4	3.5
	$^4A_1$	−0.2	3.6						
Mo	$^7A_1$	−0.1	4.9	$^5A'$	+0.1	5.1	$^5A'$	+0.3	4.7
	$^5A_1$	−0.1	4.9						
Tc	$^6A_1$	−0.1	5.9	$^4A'$	+0.1	6.0	$^4A'$	+0.3	5.9
	$^4B_1$	−0.1	6.1						
Ru	$^3A_1$	0.0	7.8	$^3A'$	+0.1	7.6	$^3A'$	+0.2	7.1
	$^5B_2$	−0.1	6.9						
Rh	$^2A_2$	0.0	8.6	$^2A'$	+0.1	8.4	$^2A'$	+0.1	8.2
	$^4A_1$	−0.1	7.9						
Pd	$^1A_1$	0.0	9.9	$^1A'$	+0.1	9.4	$^1A'$	+0.2	9.2

[a] The geometry for the η^2-complex is taken from the low-spin rhodium η^2-complex.

low-spin state of the rhodium system. For those metals which were found to have unbound η^2-complexes at this particular geometry there might be a minimum on the potential surface for longer metal–methane distances, but these minima have to be very weakly bound, probably not by more than about 2 kcal/mol. This estimate is obtained from comparison with the bonding of the H_2O molecule to a neutral nickel atom. For the H_2O molecule, which has a polarizability of the same order of magnitude as CH_4, the dispersion contribution to the binding energy is found to be about 2 kcal/mol,[30] and for the neutral metal–CH_4 systems this should be the main contribution to the bonding.

Y, Zr, Nb. The results for these metals are presented in Figure 1. The shapes of the potential curves are to a large extent determined by the low lying $4d^n5s^2$ atomic state, which is the ground state for yttrium and zirconium and only 4 kcal/mol (exp.) above the ground state for niobium. A low-lying $4d^n5s^2$ state implies that also the $4d^n5s^1p^1$ state is relatively low in energy. The product $MHCH_3$ is fairly strongly bound, by 7–12 kcal/mol, relative to the atomic ground state, and the strong bonding is achieved by a mixture of the $4d^n5s^1p^1$ and the $4d^{n+1}5s^1$ states. This mixture of states can be seen both from the Mulliken populations (see Table III) and from the structure of the $MHCH_3$ complexes, which for these metals have unusually large H–M–C angles, around 120°, indicating the importance of the $4d^n5s^1p^1$ state which in a pure form gives rise to a linear structure. Pure bonding to the $4d^{n+1}5s^1$ state would give a 90° bond angle. The increasing importance of the $4d^{n+1}5s^1$ state in the sequence Y < Zr < Nb as seen from the 4d populations in Table III, corresponds directly to the trend in atomic excitation energy for this state relative to the $4d^n5s^2$ state. Yttrium has the highest excitation energy to the $4d^{n+1}5s^1$ state, and thus the lowest involvement of this state, while for niobium the $4d^{n+1}5s^1$ state is actually the ground state, giving rise to the largest involvement of this state in the product complex.

The metals yttrium, zirconium, and niobium have high barriers for the insertion reaction, 30–40 kcal/mol, and the energy in the η^2-region, with the geometry taken from the rhodium η^2-complex, is fairly high. Both these results are effects of the large repulsion of the two 5s electrons in the $4d^n5s^2$ state. The energy in the η^2-region, using the optimal geometry for the rhodium η^2-complex, was calculated for spin states correlating with the product complexes, and these energies are marked in Figure 1. In both the transition state region and the η^2-region the highly excited low-spin coupled $4d^{n+1}5s^1$ state is mixed in to reduce the repulsion, and this is achieved through the formation of sd-hybrids. For niobium a sextet state, correlating with the $^6D(4d^45s^1)$ ground state of the atom has the lowest energy in the η^2-complex region. The excited $4d^{n+2}$ state is mixed in to reduce the repulsion.

Mo, Tc. The results for these metals are presented in Figure 2. The shapes of these potential curves are to a large extent determined by the large loss of exchange energy upon both bond formation and low-spin coupling of atomic d-electrons.[31] The product complexes, dominated by the low-lying $4d^{n+1}5s^1$ configuration (ground state for molybdenum and only 9 kcal/mol (exp) excited for technetium), are therefore fairly strong unbound, by 13–27 kcal/mol, relative to the high-spin ground states of the atoms. Relative to the low-spin coupled (i.e., the same spin as the product complexes) excited states, however, these metals have rather strongly bound insertion products, particularly for molybdenum, with a bond strength of 19 kcal/mol. Technetium is about 15 kcal/mol less bound than molybdenum, which is at least partly explained by the fact that the bonding $4d^{n+1}5s^1$ state is an excited state for technetium, while it is the ground state for molybdenum.

Both technetium and molybdenum have high insertion barriers relative to the high spin ground states, almost 50 kcal/mol, which is due both to the large loss of exchange energy and the fact that the less repulsive atomic $4d^{n+2}$ state is very high in energy. Relative to the low-spin coupled atomic asymptote, however, the barriers are significantly lower, 7–16 kcal/mol. The energy in the η^2-region, with the geometry taken from the rhodium η^2-complex, is also fairly high for these metals, which is explained by the same factors that give rise to the high barriers. Calculations in this region, using the geometry of the rhodium η^2-complex, were performed for both a high-spin state and a low-spin state, and the energies are shown in Figure 2. The high-spin states of the η^2-structures are lower than the low-spin states, which is the same order as for the atoms, but the splitting between the spin states is significantly lower for the η^2-structures. This shows that the formation of sd hybrids, which can only be done by the low-spin coupled $4d^{n+1}5s^1$ states, is important to decrease the repulsion in this region.

Ru, Rh, and Pd. The results for these metals are presented in Figure 3. These are the metals with the lowest insertion barriers, 12–24 kcal/mol relative to the atomic ground states. For rhodium and ruthenium, which have high-spin atomic ground states the barriers on the same spin-surface as the product complexes are even lower, −1 kcal/mol for rhodium and only 4 kcal/mol for ruthenium. The shapes of the potential surfaces for these three metals are to a large extent determined by the interaction between the $4d^{n+1}5s^1$ and $4d^{n+2}$ states, and since the splitting between these two states is rather different for the three metals, also the three potential surfaces are rather different from each other. Palladium and rhodium have low lying $4d^{n+2}$ states, which is the least repulsive state since it has no 5s electrons, and therefore these two metals have the lowest addition barriers. For palladium, however, the $4d^{n+1}5s^1$ state is rather high in energy and therefore the product complex is quite unstable. For rhodium the $4d^{n+1}5s^1$ state is the ground state and the product complex therefore is bound, even relative to the high-spin ground state asymptote. For ruthenium the $4d^{n+2}$ state is relatively high in energy, compared to the two other metals in Figure 3, and this explains why ruthenium has the highest barrier of the three metals. The population analysis in Table III shows that in the transition state region the $4d^{n+1}5s^1$ and the $4d^{n+2}$ states are mixed with about the same weight, while in the product region the $4d^{n+1}5s^1$ state dominates, with some admixture of the $4d^{n+2}$ state. The fact that rhodium is so much stronger bound than ruthenium, about 15 kcal/mol, although the two metals have the same $4d^{n+1}5s^1$ ground state, is explained by

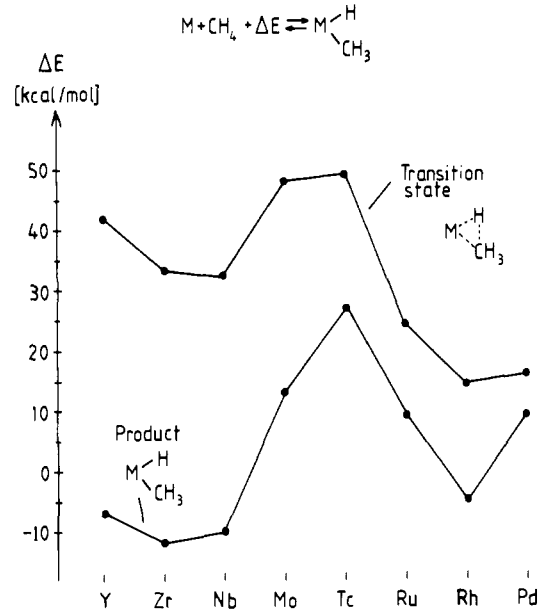

Figure 4. Relative energies for the transition state structures (upper curve) and the product complexes (lower curve), calculated relative to the ground state of the metal atom and free methane. The upper curve corresponds to the addition barrier and a large positive value for ΔE corresponds to a high activation barrier. The lower curve corresponds to the binding energy of the product complex and a large positive value for ΔE corresponds to a strongly endothermic addition reaction, while a negative value for ΔE corresponds to an exothermic addition reaction.

the lower loss of exchange energy upon bond formation for rhodium. Further, as can be seen from the populations in Table III mixing of the $4d^{n+1}5s^1$ and the $4d^{n+2}$ states is of some importance also for the bonding in the product region. In summary, rhodium is the most efficient second row metal for C–H insertion, which is a consequence of the particular atomic spectrum of rhodium with low-lying $4d^{n+1}5s^1$ and $4d^{n+2}$ states.

All these three metals have bound η^2-complexes on the low-spin potential surfaces. For all metals, calculations were only performed in the geometry optimized for the rhodium η^2-complex. Using this geometry the ruthenium and rhodium η^2-complexes are bound by 12 and 9 kcal/mol, respectively, relative to the excited low-spin atomic asymptotes. The palladium η^2-complex is bound by 4 kcal/mol relative to the singlet atomic ground state, and palladium is the only metal for which the η^2-complex has the lowest energy on the ground state potential surface. The population analysis shows that the $4d^{n+2}$ state dominates in this region, with important admixture of the $4d^{n+1}5s^1$ states.

III. Discussion

In this section the results of the calculations will be discussed in the context of different types of experimental information. The main motivation for the present study is to contribute to the understanding of the mechanisms of C–H activation in homogenous catalysis where the active catalysts are ligated complexes. Below we will discuss how to best make comparisons between the naked atom model presently used and the conclusions drawn from experimental information for the ligated metal complexes. Comparisons will also be made between the present calculations and experimental information about the reactivity of naked metal atoms.

To simplify the comparisons between the metals, the reaction energies (binding energies and barrier heights) for all second row metals are plotted in Figure 4. From this figure it can be seen that among the second row transition metal atoms rhodium has the lowest barrier for C–H addition and palladium has the lowest barrier for C–H elimination.

The result that the rhodium atom has the lowest barrier for insertion into the C–H bond in methane is in good accord with the fact that rhodium complexes, to our knowledge, are the only second row transition metal complexes experimentally observed

Table IV. Calculated Relative Energies (in kcal/mol) for the Reaction between Methane and Different Models of a Rhodium Complex[a]

model	ref state	η^2-complex state	η^2-complex ΔE	transition state state	transition state ΔE	insertion product state	insertion product ΔE
$ClRh(PH_3)_2$	$^1A_1$	$^1A_1$	−12	$^1A_1$	−2	$^1A_1$	−10
Rh^+	^3F	$^3A_2$	−13	$^3A'$	11	$^1A'$	24
Rh	^4F	$^2A_2$	6	$^2A'$	14	$^2A'$	−5
Rh	^2D	$^2A_2$	−9	$^2A'$	−1	$^2A'$	−19

[a] For the neutral naked metal atom model, two different states are used as reference point, the ground ^4F state and the lowest low-spin ^2D state.

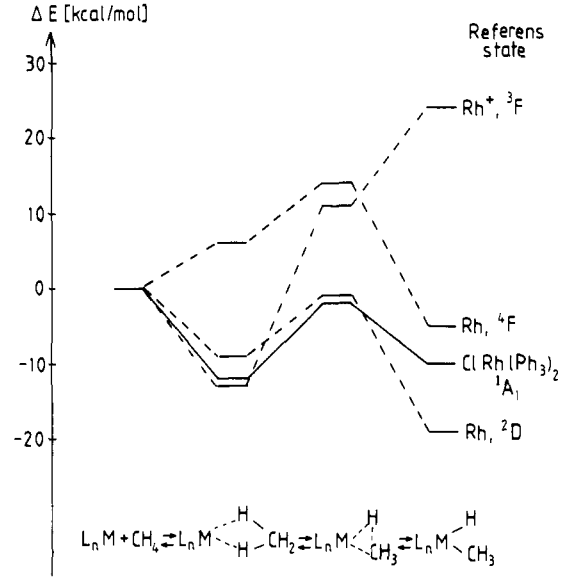

Figure 5. Relative energies for the reaction between methane and different models of a rhodium complex. For the neutral naked metal atom model, two different states are used as reference point.

to activate alkane C–H bonds by the oxidative addition mechanism in solution[3,4] and in matrices.[6–8] It is unlikely that this is just a coincidence, and, to examine more in detail, differences and similarities between ligated metal complexes and naked metal atoms calculations were performed also for the reaction between methane and the rhodium complex $ClRh(PH_3)_2$. This complex is chosen to model the $ClRh(PPh_3)_2$ complex, which is believed to be active in an experimentally observed C–H insertion process.[4] This model system has been used previously in a theoretical study by Koga and Morokuma.[27] The same four points on the potential surface as for the naked metal atoms were calculated for the $ClRh(PH_3)_2$ complex. The results are summarized in Table IV and Figure 5, where also the reaction energies for the naked rhodium atom have been included, using two different reference points, the high-spin ground state and the low-spin excited state corresponding to the state of the insertion product. Another aspect of the comparison between metal atoms and metal complexes is the oxidation state of the metal. The neutral naked metal atom has the oxidation state zero, while in the reacting metal complexes higher oxidation states are common. One simple way to obtain correct oxidation states for the naked atom model is to use cations instead of neutral atoms, with a charge corresponding to the oxidation state of the metal in a particular type of complexes. Rh^+ could thus be used to model the Rh(I) in the $ClRh(PH_3)_2$ complex. In Table IV and Figure 5 we have therefore also included the reaction energies for the naked rhodium cation using the same geometries as for the neutral atom.

Comparing the $ClRh(PH_3)_2$ complex with the different naked atom models in Table IV and Figure 5 it can be seen that the best overall agreement with the ligated complex is obtained for the neutral atom following the low-spin surface. In the region of the η^2-complex both the cation and the low-spin rhodium atom give

results close to the full complex. For the cationic system, the η^2-complex is bound by 13 kcal/mol, and the attraction between rhodium and the methane molecule is dominated by the charge-induced dipole interaction. For the neutral rhodium atom, as discussed in the previous section, the low-spin coupling of the valence electrons is crucial for the formation of an η^2-complex, the low-spin η^2-complex is bound by 9 kcal/mol relative to the low-spin asymptote, while on the high spin surface there is no minimum for the η^2-structure. For the ligated complex the binding energy of the η^2-structure is 12 kcal/mol, and the binding can be viewed as a combination of the type of binding in the neutral atomic low-spin complex and the pure electrostatic binding of the cationic complex. In the region of the insertion product the ligated complex is bound by 10 kcal/mol. For the neutral rhodium atom the product complex is bound by as much as 19 kcal/mol relative to the low-spin asymptote and by 5 kcal/mol relative to the high-spin ground state, while for the cation there is no minimum for the product complex and the energy in this region is 24 kcal/mol above the asymptote. Thus, for the product complex only the neutral atom gives results reasonably close to the ligated complex. Also in the region of the transition state the low-spin coupled neutral atom gives the best correspondence to the full complex with a relative energy of −1 kcal/mol compared to −2 kcal/mol for the ligated complex. It is interesting to compare the present results with those obtained for the same system by Koga and Morokuma[27] using effective core potentials (ECP) to describe the inner shell electrons and Möller–Plesset perturbation theory (MP4) to describe electron correlation effects. Qualitatively the presently obtained potential surface is quite similar to the one obtained by Koga and Morokuma, but their surface is everywhere more attractive, in particular in the product region where the difference is as large as 14 kcal/mol. Koga and Morokuma obtain the η^2-complex bound by 18 kcal/mol, the product complex by 24 kcal/mol, and the transition state below the asymptote by 14 kcal/mol. The corresponding values obtained in the present study are 12, 10, and 2 kcal/mol, respectively. In the transition state and the product regions two sets of test calculations were performed to evaluate the accuracy of the presently obtained results. First, the effects of f-functions on rhodium in the atomic basis set was investigated, which was found to change the relative energies by less than 0.5 kcal/mol. Second, the correlation effects were tested by using the coupled cluster method (CCSD(T)),[32] and the relative energies of the transition state structure and the product complex were in this case lowered by about 3 kcal/mol. This leads us to conclude that our results should be reliable to within about 5 kcal/mol. The too attractive potential surface obtained by Koga and Morokuma is probably explained both by the use of a rhodium ECP replacing also the outermost core orbitals which has been shown to be unreliable[25] and by the use of the Möller–Plesset perturbation theory for correlation effects, which has been found to sometimes lead to spurious results for transition metal systems.[33]

Thus the fact that the neutral rhodium atom for a large part of the potential surface gives the best correspondence to the ligated Rh(I) complex shows that the oxidation state of the metal does not appear to be very important in modelling the metal complex. In particular, for higher oxidation states a multiply charged metal atom is not expected to be a good model of the metal complex, since from quantum chemical studies it is well-known that a high oxidation state of a metal atom in a complex does not correspond to a positive metal charge of that magnitude. In fact, the charge on a metal in a neutral complex is seldom larger than one, which is in accord with the Pauling electroneutrality principle.[34]

The fact that the excited low-spin state of the rhodium atom yields the best correspondence to the potential surface of the full complex is perhaps not very surprising, since the coordinatively unsaturated metal fragment, $ClRh(PH_3)_2$, that is reacting with the hydrocarbon is assumed to be in its low-spin state. In the present calculations the low-spin (singlet) state of $ClRh(PH_3)_2$ is an excited state. The ground triplet state is found to be about 3 kcal/mol lower than the singlet state. However, such a small calculated splitting between a triplet and a singlet state indicates that the actual ground state of the metal fragment might very well be the singlet state, since usually a more accurate description of correlation effects will decrease the energy of the singlet state relative to the triplet state. This splitting between the high-spin ground state and the low-spin excited state of the ligated rhodium complex of 3 kcal/mol or less should be compared to the calculated splitting of 15 kcal/mol between the high-spin ($^4F(4d^85s^1)$) and low-spin ($^2F(4d^85s^1)$) states of the rhodium atom. In general the ligands on the metal complex will stabilize the low-spin states, and the excitation energies to the low-spin states of the metal complexes are therefore expected to be lower than for the free metal atoms. For the CpRhL fragment ($L = C_2H_4$) the spin state has been investigated experimentally, and the results strongly suggest a singlet ground state.[7] Therefore, for rhodium the low-spin surfaces for the naked atom are expected to be closer to the ligated complexes than if the ground state high-spin is used as reference point. However, in particular for the metals with very large splittings between the spin states it is not expected that the atomic excited low-spin state should give potential surfaces as close to the ligated metal complexes as was found in the rhodium case. In summary, the reactivity of a certain metal complex is probably best estimated by considering both the ground state and the low-spin reference points for the naked metal atom model. It is further interesting to note that among the second row metals, rhodium will have the lowest barrier for insertion into the C–H bond of methane whichever of these two approaches is followed. Using the high-spin ground state as reference point leads to an insertion barrier of only 14 kcal/mol for rhodium, followed by palladium and ruthenium with barrier heights of 16 and 24 kcal/mol, respectively. Following the low-spin surface, rhodium is the only metal without a barrier. The second lowest barrier is obtained for ruthenium with a value of 4 kcal/mol.

Turning now to the experiments performed for naked metal atoms, the comparison between the calculated results and experiment is obviously more direct since no modelling is involved. For neutral metal atoms there are rather few experiments performed to elucidate their reactivity toward saturated hydrocarbons. In an early study Klabunde and Tanaka[12a] showed that many ground state metal atoms (including the second row atoms Pd and Ag) were unreactive toward methane under matrix conditions. The only metal atom found to be reactive was aluminum. Ritter and Weisshar[13] have found no reactivity for a sequence of first row transition metal atoms with linear alkanes. For rhodium[35] and palladium,[36] cluster experiments have shown no reaction between a single metal atom and methane. In a recent study Klabunde et al.[12b] have investigated the reactivity of all transition metal atoms toward methane and in contrast to previous results found the following second row atoms to be strongly interacting with methane: niobium, molybdenum, ruthenium, rhodium, and silver. Zirconium and palladium were found to be moderately interacting, while yttrium was only weakly interacting with methane. It should, however, be noted that among the second row metals, the insertion product $MHCH_3$ was only identified for the case of rhodium.

The present results for the neutral atoms show that for yttrium to technetium the reaction barriers for ground state insertion into the C–H bond of methane are larger than about 30 kcal/mol. The lowest barriers are found for rhodium (14 kcal/mol) and palladium (16 kcal/mol), but for palladium the product complex is unbound by 9 kcal/mol. Also for ruthenium, with an intermediate barrier

(30) Bauschlicher, C. W., Jr. *Chem. Phys. Lett.* **1987**, *142*, 71.
(31) Carter, E. A.; Goddard III, W. A. *J. Phys. Chem.* **1988**, *92*, 5679.
(32) The coupled cluster calculations are performed using the TITAN set of electronic structure programs, written by Lee, T. J., Rendell, A. P., Rice, J. E..
(33) Blomberg, M. R. A.; Brandemark, U. B.; Siegbahn, P. E. M.; Wennerberg, J.; Bauschlicher, Jr., C. W. *J. Am. Chem. Soc.* **1988**, *110*, 6650.
(34) Collman, J. P.; Hegedus, L. S.; Norton, J. R.; Finke, R. G. *Principles and Applications of Organotransition Metal Chemistry*; University Science Books: Mill Valley, CA, 1987.
(35) Zakin, M. R.; Cox, D. M.; Kaldor, A. *J. Chem. Phys.* **1988**, *89*, 1201.
(36) Fayet, P.; Kaldor, A.; Cox, D. M. *J. Chem. Phys.* **1990**, *92*, 254.

of 24 kcal/mol, the product complex is unstable by 9 kcal/mol. Thus rhodium, having a stable product complex, bound by 6 kcal/mol, is the second row transition metal for which insertion into the C–H bond of methane is most likely to be observed. Still, an activation energy of about 0.5 eV is required and also a spin transition, from the quartet ground state of the atom to the doublet ground state of the insertion product. We therefore conclude that there must be some other explanation for the most recent observations made by Klabunde et al.,[12b] in experiments performed at very low energies (10–20 K), than the insertion of ground state metal atoms into the C–H bond of methane. Perhaps excited states of the metal atoms are involved. It should further be noticed that for palladium the lowest point on the ground state potential curve is the molecular η^2-complex, bound by about 4 kcal/mol, making palladium unique among the second row atoms in that it is the only one that has a bound η^2-complex on the ground state potential surface.

IV. Conclusions

The insertion of a second row transition metal atom into the C–H bond of methane proceeds in all cases with the appearance of an energy barrier. This barrier is a result of an avoided crossing between two potential surfaces. Outside the barrier, where methane approaches the metal atom, the potential surface is essentially repulsive for most of the metals. The main exception is palladium, which forms a bound precursor complex with methane on the ground state potential surface, with a binding energy of 4 kcal/mol. Other exceptions are rhodium and ruthenium which form rather strongly bound (9–12 kcal/mol) complexes with methane on their low-spin surfaces. The shape of the potential surface outside the barrier, including the precursor region, is determined by how repulsive the atomic state of the metal is. The least repulsive state is the d^{n+2} state which is the ground state for palladium and a low-lying state for rhodium and ruthenium. Inside the barrier, where the insertion complex is formed, the shape of the potential surface is determined by the strength of the covalent bonds that are formed. To form the required two covalent bonds, a state on the metal with two open shells is required. The lowest lying state for all the second row transition metal atoms, which can form two covalent bonds is the $d^{n+1}s$ state. When this state is the ground state a strongly bound insertion complex is expected. This is the case for rhodium, ruthenium, and niobium. For the metals to the left the d^ns^2 state is the ground state, which implies that the $d^ns^1p^1$ state is rather low in energy and can also contribute to the bonding. For the atoms in the middle of the row the loss of exchange energy is also an important factor. In particular for molybdenum, which has all the 4d electrons with parallel spin in the ground state, the formation of a 4d bond leads to a large loss of exchange energy. Even though molybdenum has a $d^{n+1}s$ ground state, which should be favorable for strong bond formation, this exchange energy loss leads to an insertion complex with weak bonds.

A low barrier for the C–H insertion reaction will be obtained when the repulsion is low outside the barrier and the bonds in the insertion complex are strong. According to the above analysis the requirement on the metal atom is thus that both the d^{n+2} and the $d^{n+1}s$ states are low lying states. This requirement is best fulfilled for the atoms to the right of the row, i.e., for ruthenium, rhodium, and palladium. The optimal situation occurs for rhodium which has a $d^{n+1}s$ ground state and where the excitation energy to the d^{n+2} state is only 8.1 kcal/mol (exp). Palladium has a d^{n+2} ground state, but the excitation energy to the $d^{n+1}s$ state is as high as 21.9 kcal/mol (exp). This leads to low repulsion in the entrance channel but to weak bonds in the insertion complex, which is more favorable for the reverse reaction, reductive elimination, where palladium has the lowest barrier of all the metals studied.

Even though the reaction of naked metal atoms with methane is of interest as such, a critical question for a study of the present type is how relevant naked atoms are as models for a piecewise understanding of the reactivity of real ligated complexes. In the present study there are particularly two results which support this type of modelling. The first result is that the lowest barrier for the insertion reaction is found for rhodium, which agrees with the fact that the only second row transition metal complexes which have been found experimentally to activate alkane C–H bonds by the oxidative addition mechanism are rhodium complexes. These results are unlikely to be just a coincidence, and the conclusion must be that the position of the atomic states of the transition metal is of considerable interest and relevance when the reactivity of ligated complexes are discussed and analyzed. The other positive result in this context is that the potential surface of the rhodium atom and methane is found to be remarkably similar to the potential surface of $ClRhL_2$ and methane. The latter compound is one of the few compounds that has been found to activate alkanes experimentally.[4] Another interesting result for the latter reaction is that the η^2 complex is found to be so strongly bound, by 12 kcal/mol relative to the separated fragments, which may have been unexpected.

Another type of model reaction, where there are many more experimental results available, is the reaction between transition metal cations and alkanes. Due to the positive charge on the metal, direct electrostatic effects can be expected to modify the potential surfaces considerably compared to the neutral metal reactions. Calculations of the same type as in the present study have also been performed for the whole second row transition metal cation reactions, and the results of that study will be presently shortly and will there be compared to the results of this study.

V. Appendix: Computational Details

In the calculations reported in the present paper for the reaction of methane with the second row transition metal atoms large basis sets were used in a generalized contraction scheme,[37] and all valence electrons were correlated. Relativistic effects were accounted for using first order perturbation theory including the mass velocity and Darwin terms.[38]

For the metal atoms the Huzinaga primitive basis[39] was extended by adding one diffuse d-function, two p-functions in the 5p region, and three f-functions, yielding a (17s, 13p, 9d, 3f) primitive basis. The core orbitals were totally contracted except for the 4s and 4p orbitals which have to be described by at least two functions each to properly reproduce the relativistic effects.[40] The 5s and 5p orbitals were described by a double-ζ contraction and the 4d by a triple-ζ contraction. The f functions were contracted to one function giving a [7s, 6p, 4d, 1f] contracted basis. Some spectroscopic results for the atoms using these basis sets are given in Table II.

For carbon the primitive (9s, 5p) basis of Huzinaga[41] was used, contracted according to the generalized contraction scheme to [3s, 2p]. In most calculations one d function with exponent 0.63 was added on carbon. For the active hydrogen the primitive (5s) basis from ref 41 was used, augmented with one p function with exponent 0.8, and contracted to [3s, 1p]. The inactive methyl hydrogens were described by the (4s) basis from ref 41 contracted to [2s] and with the exponents scaled by a factor 1.2. In the calculations on the $ClRh(PH_3)_2$ complex the (12s, 9p) uncontracted basis of ref 42 was used for Cl and P, contracted to [4s, 3p]. For chlorine one diffusion p-function with exponent 0.044 was added leading to a [4s, 3p] contracted basis. The phosphine hydrogens were described by the same basis set as the inactive methyl hydrogens.

The correlated calculations were performed using the modified coupled pair functional (MCPF) method,[43] which is a size-consistent, single reference state method. For the low-spin coupled states of the atoms and the precursor complex, which cannot be

(37) (a) Almlöf, J.; Taylor, P. R. *J. Chem. Phys.* **1987**, *86*, 4070. (b) Raffenetti, R. C. *J. Chem. Phys.* **1973**, *58*, 4452.
(38) Martin, R. L. *J. Phys. Chem.* **1983**, *87*, 750. See, also: Cowan, R. D.; Griffin, D. C. *J. Opt. Soc. Am.* **1976**, *66*, 1010.
(39) Huzinaga, S. *J. Chem. Phys.* **1977**, *66*, 4245.
(40) Blomberg, M. R. A.; Wahlgren, U. *Chem. Phys. Lett.* **1988**, *145*, 393.
(41) Huzinaga, S. *J. Chem. Phys.* **1965**, *42*, 1293.
(42) Huzinaga, S. *Approximate Atomic Functions, II*; Department of Chemistry Report, University of Alberta, Edmonton, Alberta, Canada, 1971.
(43) Chong, D. P.; Langhoff, S. R. *J. Chem. Phys.* **1986**, *84*, 5606.

Table V. Geometries Used in the Calculations[a]

	M-C [a_0]	M-H [a_0]	∠CMH insertion product	∠CMH transition state
Y	4.52	3.77	118°	40°
Zr	4.41	3.64	120°	40°
Nb	4.31	3.50	124°	41°
Mo	4.17	3.30	120°	40°
Tc	4.05	3.15	120°	40°
Ru	3.91	3.02	100°	43°
Rh	3.83	2.80	83°	48°
Pd	3.68	2.87	80°	51°

[a] For each metal the same bond lengths are used for the $HMCH_3$ insertion product and the transition state structure. For the choices of geometries see the discussion in the Appendix.

described by a single reference determinant, the average coupled pair functional (ACPF) method[44] was used. The metal 4d and 5s electrons and all electrons on the CH_4 unit except the C 1s were correlated. In the calculations on the $ClRh(PH_3)_2$ complex all valence electrons on the Cl and PH_3 ligands were also correlated.

The geometry optimizations were performed using slightly smaller basis sets than those described above. On the metal atoms the f-function was deleted, and on carbon the d-function was taken away. The internal methyl structure was kept frozen in all calculations with the C-H bond fixed to 2.082 a_0 and the H-C-H angle to 107.8°. For the molecularly bound methane complex the η^2-structure optimized in ref 25 for the neutral rhodium atom was used for all metals, since the energy is rather insensitive to the exact geometry in this region. The metal-carbon distance used in the η^2-complex is 4.72 au. The geometries for the insertion product and the transition state were partially optimized for most of the metals in the following way. In all cases the metal-carbon and metal-hydrogen distances at the transition state were taken to be the same as for the insertion product. For the palladium system this restriction was found to increase the barrier height by less than 1 kcal/mol (compare ref 24). For yttrium, niobium, and ruthenium the geometries were optimized at the SCF level. The methyl tilt angle was kept at 0° for the $HMCH_3$ insertion product and at 25° for the transition state. Thus, for these metals, the metal-carbon and metal-hydrogen distances, together with the C-M-H angle, were optimized for the insertion product, while for the transition state only the C-M-H angle was optimized. For the rhodium system the geometry of the insertion product was taken from the optimized structure in ref 27. For the transition state of the rhodium system a two-dimensional optimization was performed for the C-M-H bend angle and the methyl tilt angle at both the SCF and the MCPF level. Only the bend angle changed between these two optimizations, and a value of 46° was obtained at the SCF level and 41° at the MCPF level. The energy difference between these two geometries at the MCPF level was only 0.2 kcal/mol, showing that the SCF optimizations should give reliable results. For the palladium system the geometries of the insertion product and the transition state were taken from the optimized structures in ref 22b, with the only modification that the bond distances to the metal in the transition state were taken to be the same as for the insertion product. This modification was made to obtain an equivalent treatment for all the metals. Finally, for zirconium, molybdenum, and technetium the geometries of both the insertion products and the transition states were extrapolated from the above described optimized structures. The geometrical parameters used are summarized in Table V. The errors in relative energies introduced by the nonoptimal geometries are estimated to be on the order of a few kcal/mol.[24,25]

(44) Gdanitz, R. J.; Ahlrichs, R. *Chem. Phys. Lett.* **1988**, *143*, 413.

Registry No. Y, 7440-65-5; Zr, 7440-67-7; Nb, 7440-03-1; Mo, 7439-98-7; Tc, 7440-26-8; Ru, 7440-18-8; Rh, 7440-16-6; Pd, 7440-05-3; CH_4, 74-82-8; $HYCH_3$, 141223-15-6; $HZrCH_3$, 141223-16-7; $HNbCH_3$, 141223-17-8; $HMoCH_3$, 141223-18-9; $HTcCH_3$, 141223-19-0; $HRuCH_3$, 141223-20-3; $HRhCH_3$, 141223-21-4; $HPdCH_3$, 93895-87-5.

Transition-Metal Polyhydride Complexes. 3. Relative Stabilities of Classical and Nonclassical Isomers

Zhenyang Lin and Michael B. Hall*

Contribution from the Department of Chemistry, Texas A&M University, College Station, Texas 77843. *Received November 26, 1991*

Abstract: Ab initio calculations with effective core potentials have been used to study the relative stabilities of classical and nonclassical isomers of 18-electron polyhydride transition-metal complexes. Systematic calculations on $ML_{7-n}H_n$ and $ML_{8-n}H_n$ (n = 2-7), where M = Mo, W, Tc, Re, Ru, Os, Rh, and Ir, and L = PH_3 and CO, lead to the following conclusions. The trans influence of two H ligands is significantly destabilizing and influences the stability and structure of the isomers. A diagonal line in the Periodic Table through Ru and Ir divides the classical (left side of the line) and nonclassical (right side of the line) forms for neutral complexes without strong π-accepting ligands. For monocationic hydride complexes the corresponding diagonal line shifts slightly toward early transition metals and crosses between Tc/Ru and Os/Ir. The stability of nonclassical complexes increases with an increase in the number of strong π-accepting ligands or with an increasing contraction of the transition-metal d orbitals. The conclusion for cationic hydride complexes applies to neutral polyhydride transition-metal complexes with a chloride ligand because of the strong electron-withdrawing ability of chloride. Our calculations predict that several complexes previously identified as nonclassical isomers should be reclassified as classical isomers. The trends predicted here also lead to suggestions for finding new classical and nonclassical isomers.

Introduction

Transition-metal polyhydride complexes have been the subject of considerable interest[1-27] since the first discovery of a stable nonclassical dihydrogen complex, $W(CO)_3[P(i\text{-}Pr)_3]_2(\eta^2\text{-}H_2)$, by Kubas et al. It is now clear that polyhydrides may adopt classical

(1) (a) Kubas, G. J.; Ryan, R. R.; Swanson, B. J.; Vergamini, P. J.; Wasserman, H. J. *J. Am. Chem. Soc.* **1984**, *106*, 451. (b) Kubas, G. J.; Ryan, R. R.; Wroblewski, D. *J. Am. Chem. Soc.* **1986**, *108*, 1339. (c) Kubas, G. J.; Unkefer, C. J.; Swanson, B. J.; Fukushima, E. *J. Am. Chem. Soc.* **1986**, *108*, 7000. (d) Kubas, G. J. *Acc. Chem. Res.* **1988**, *21*, 120. (e) Khalsa, G. R. K.; Kubas, G. J.; Unkefer, C. J.; van der Sluys, L. S.; Kubat-Martin, K. A. *J. Am. Chem. Soc.* **1990**, *112*, 3855.

(2) (a) Sweany, R. L. *J. Am. Chem. Soc.* **1985**, *107*, 2374. (b) Upmacis, R. K.; Poliakoff, M.; Turner, J. *J. Am. Chem. Soc.* **1986**, *108*, 3645.

(3) (a) Bautista, M. T.; Earl, K. A.; Morris, R. H.; Sella, A. *J. Am. Chem. Soc.* **1987**, *109*, 3780. (b) Bautista, M. T.; Earl, K. A.; Maltby, P. A.; Morris, R. H.; Schweitzer, C. T.; Sella, A. *J. Am. Chem. Soc.* **1987**, *109*, 3780. (c) Earl, K. A.; Polito, M. A.; Morris, R. H. *J. Am. Chem. Soc.* **1987**, *109*, 3780. (d) van der Sluys, L. S.; Eckert, J.; Eisenstein, O.; Hall, J. H.; Huffman, J. C.; Jackson, S. A.; Koetzle, T. F.; Kubas, G. J.; Vergamini, P. J.; Caulton, K. *J. Am. Chem. Soc.* **1990**, *112*, 4831.

0002-7863/92/1514-6102$03.00/0